Constraining the Photoionization Models With a Reprojected Optical Diagnostic Diagram

Xihan Ji[1]★, Renbin Yan[1]†
[1]*Department of Physics and Astronomy, University of Kentucky, 505 Rose Street, Lexington, KY 40506, USA*

Accepted XXX. Received YYY; in original form ZZZ

ABSTRACT

Optical diagnostic diagrams are powerful tools to separate different ionizing sources in galaxies. However, the model-constraining power of the most widely-used diagrams is very limited and challenging to visualize. In addition, there have always been classification inconsistencies between diagrams based on different line ratios, and ambiguities between regions purely ionized by active galactic nuclei (AGNs) and composite regions. We present a simple reprojection of the 3D line ratio space composed of [N II]λ6583/Hα, [S II]$\lambda\lambda$6716, 6731/Hα, and [O III]λ 5007/Hβ, which reveals its model-constraining power and removes the ambiguity for the true composite objects. It highlights the discrepancy between many theoretical models and the data loci. With this reprojection, we can put strong constraints on the photoionization models and the secondary nitrogen abundance prescription. We find that a single nitrogen prescription cannot fit both the star-forming locus and AGN locus simultaneously, with the latter requiring higher N/O ratios. The true composite regions stand separately from both models. We can compute the fractional AGN contributions for the composite regions, and define demarcations with specific upper limits on contamination from AGN or star formation. When the discrepancy about nitrogen prescriptions gets resolved in the future, it would also be possible to make robust metallicity measurements for composite regions and AGNs.

Key words: galaxies: active – galaxies: nuclei – galaxies: star formation

1 INTRODUCTION

The widely used optical diagnostic diagrams (hereafter BPT diagrams) originally proposed by Baldwin et al. (1981) and refined by Veilleux & Osterbrock (1987) are very useful for distinguishing among different ionization mechanisms in galaxies. The merits of these diagnostics are that only ratios of strong optical emission lines are involved (i.e. [S II]$\lambda\lambda$6716, 6731/Hα, [N II]λ6583/Hα, [O I]λ6300/Hα, and [O III]λ5007/Hβ), and they are insensitive to dust extinction. Various demarcations have been proposed based on

2000; Kewley & Dopita 2002; Groves et al. 2004b; Dopita et al. 2013).

However, there are several limitations associated with the usage of the BPT diagrams. First of all, there is often ambiguity between the classifications of different BPT diagrams. Spectra classified as AGN in one diagram could be classified as star-forming (SF) in another diagram, and vice versa. These ambiguous cases are tricky to deal with and are often excluded in data analyses, leading to biased or incomplete physical interpretations. In addition, photoion-

Идея работы и модели

- Основная идея – найти оптимальный разворот 3D-сетки моделей в пространстве параметров BPT.
- Строят сетку моделей в Starburst99 (Cont. SF > 4Myr, Kroupa IMF), разные Z, q, nHI – в CLOUDY считают эмиссионные спектры. Для AGN – модель SED из Groves(2004)
- Сравнивают с данными MaNGA DR15, но только для r<0.3Reff

Table 1. Photoionization model sets

Parameter	Values
	SF models
q	−4.0, −3.5, −3.0, −2.5, −2.0
[O/H]	−1.3, −0.7, −0.4, 0.0, 0.3, 0.5
$\log(n_H/cm^{-3})$	1.15
Ionizing SED	`Starburst99` models with $\log(Z/Z_\odot) = -1.3, -0.7, -0.4, 0.0, 0.3$
	Continuous SFH for 4 Myr
Nitrogen prescription	Dopita13 prescription
	AGN models
q	−4.0, −3.5, −3.0, −2.5, −2.0
[O/H]	−0.75, −0.5, −0.25, 0.0, 0.25, 0.5, 0.75
$\log(n_H/cm^{-3})$	2.0
Ionizing SED	power-law SED with the power-law index $\alpha = -1.4$ (fiducial), −1.7 (preferred by data)
Nitrogen prescription	Groves04 prescription

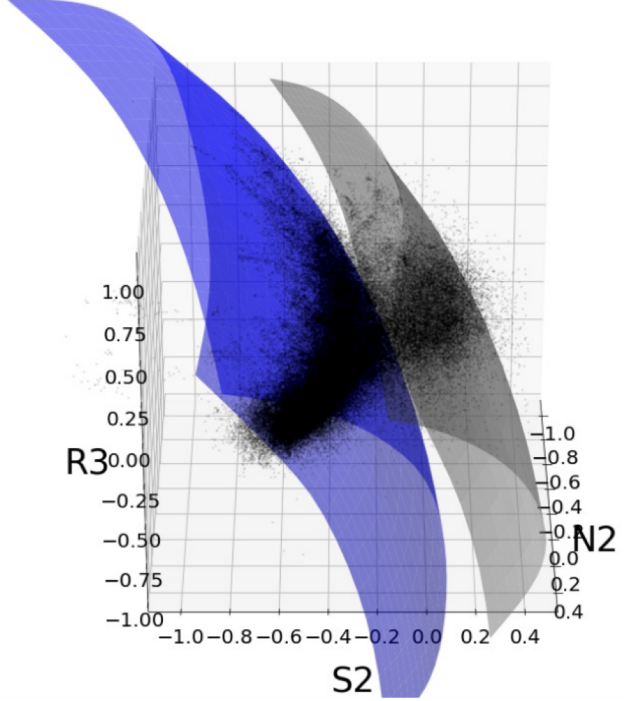
R3
S2
N2

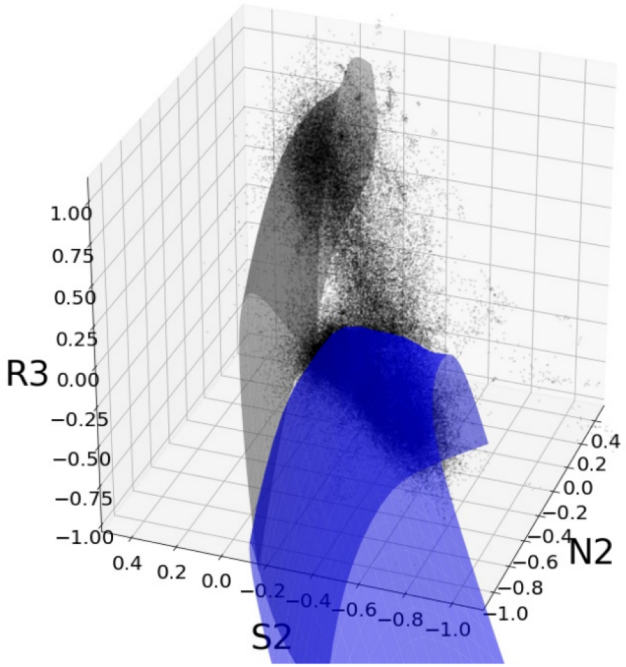
R3
S2
N2

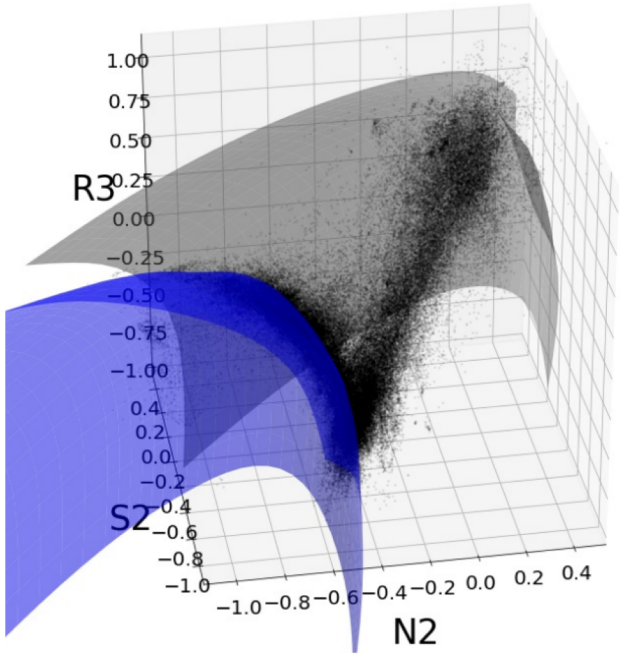
R3
S2
N2

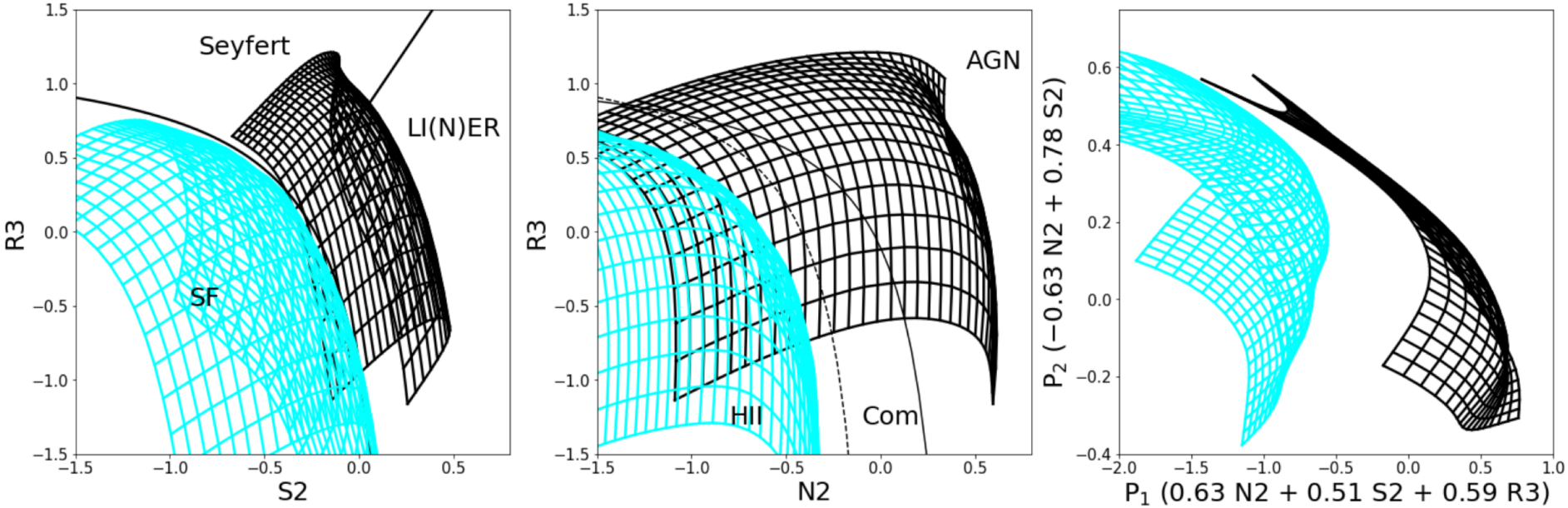

Figure 2. Comparison of photoionization models in three optical diagnostic diagrams. AGN model grids (black) and SF model grids (cyan) displayed in the diagrams have been smoothed through interpolation. Left panel: the [S II]-based BPT diagram; middle panel: the [N II]-based BPT diagram; right panel: the new diagram proposed by this paper.

В предложенной авторами проекции модели для SF и AGN прекрасно разделяются, что позволяет безошибочно отделять SF, AGN и композитные области.

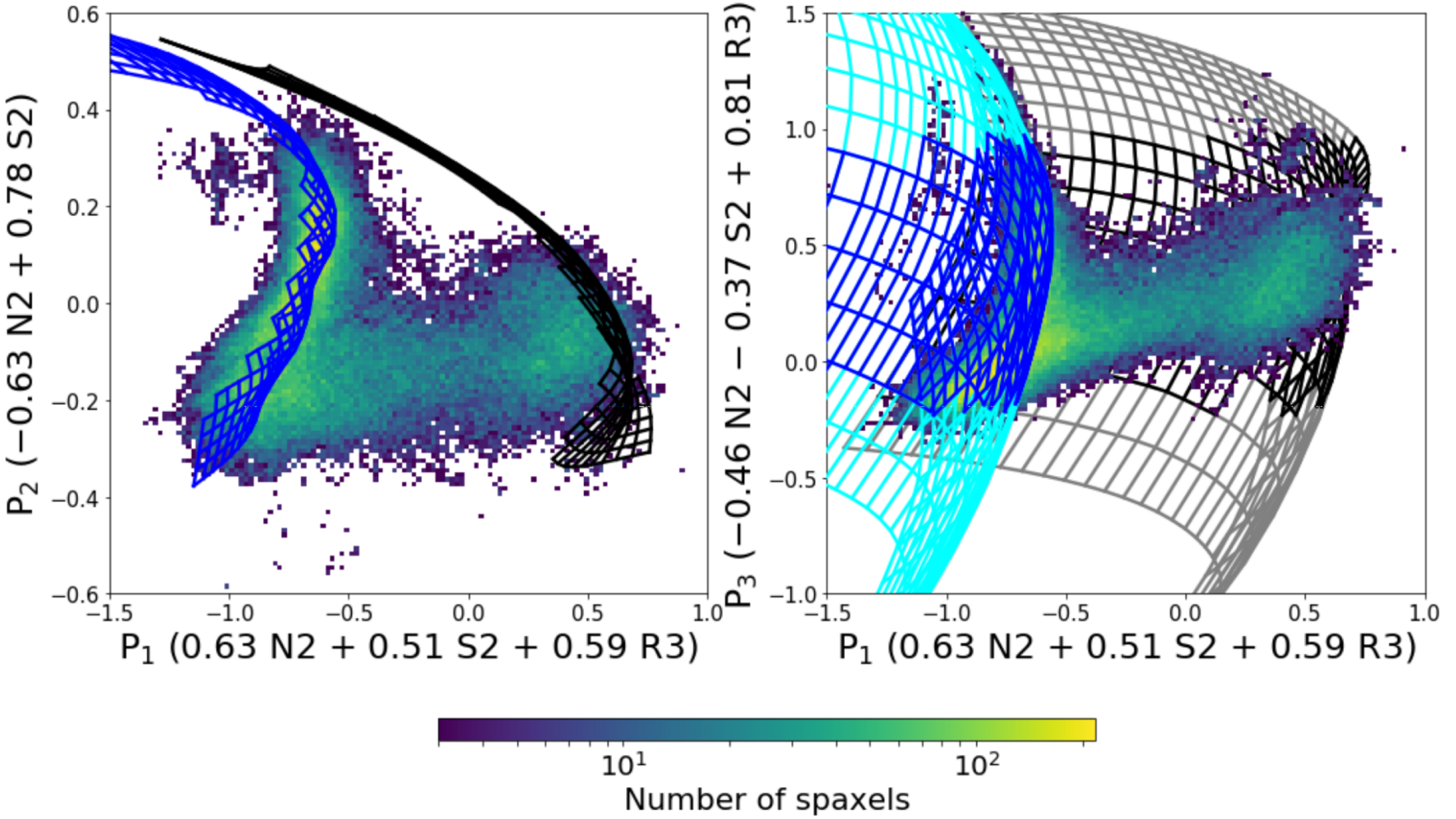

Figure 5. Left panel: final plane of projection. The photoionzation models are first interpolated and then cut in the P_3 (perpendicular) direction so that they cover the middle 98% of the data points. Right panel: $P_1 - P_3$ plane. Parts of the model grids (in cyan and grey) are cut off according to the distribution of the data points along the P_3 axis. The 2D number density distributions of the our sample spaxels are displayed in both panels.

Не очень хорошее согласие моделей AGN и основного «облака» данных для них

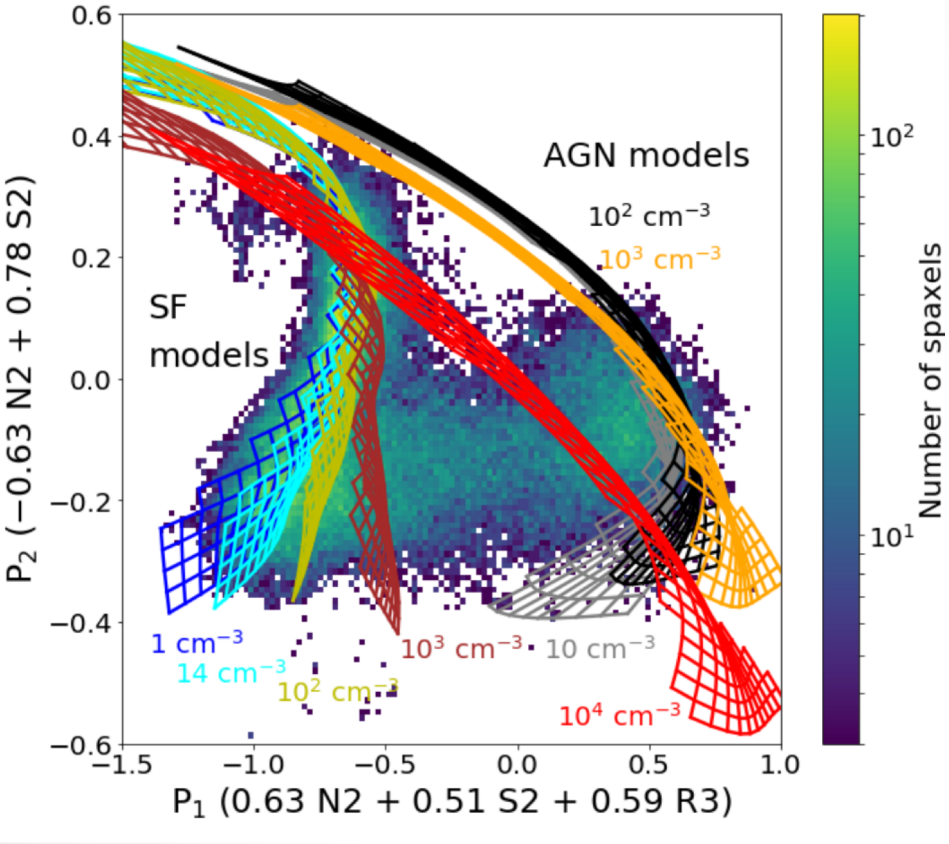

Вариация плотности не объясняет разногласие для моделей и положения AGN

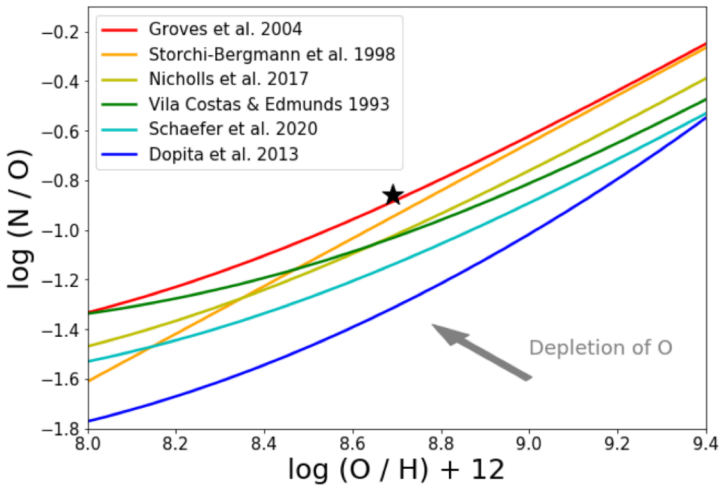

Figure 8. Various nitrogen prescriptions in literature. The Groves04 and the Dopita13 are the two prescriptions used in this paper. The solar abundance is indicated by the black star. The arrow shows the effect of the depletion of oxygen onto dust grains by 0.22 dex. By default `CLOUY` assumes that oxygen depletes by 40% or approximately 0.22 dex, while nitrogen does not deplete.

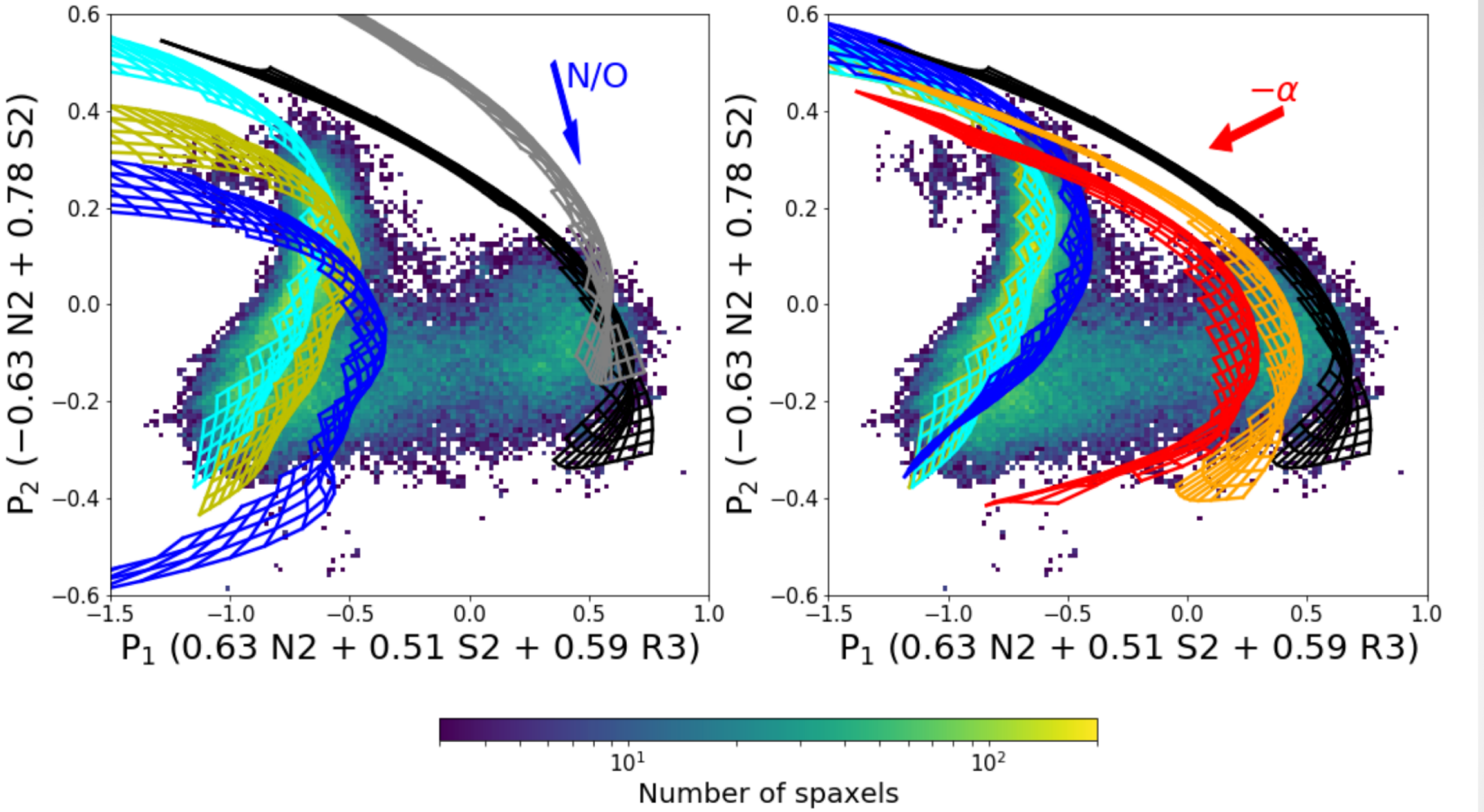

Figure 7. Photoionization model grids and the distribution of MaNGA central spaxels in the new diagram. The color-coding of the data indicates the density of spaxels in the diagram. Left panel: the SF model with the Dopita13 (Groves04) nitrogen prescription is shown in cyan (blue), and the AGN model with the Dopita13 (Groves04) nitrogen prescription is shown in grey (black). Besides these two extreme prescriptions, the Scheafer20 prescription is used to compute the yellow model grid for SF regions. The blue arrow roughly indicates how the model grids would move if the overall N/O ratio is increased. Right panel: AGN models with a Groves04 nitrogen prescription and input SEDs of which the power-law indices are −1.4, −1.7 and −2.0 are shown in black, orange, and red, respectively. The red arrow roughly indicate in what direction the AGN model grid would move if the power-law index of the input SED is decreased. SF models generated by SEDs of continuous star-formation history but different ages are plotted as well. The star-forming ages for the blue, cyan, and yellow models are 0.01 Myr, 4 Myr, and 8 Myr, respectively. All the models are cut so that they enclose the middle 98% of the data along the P_3 axis.

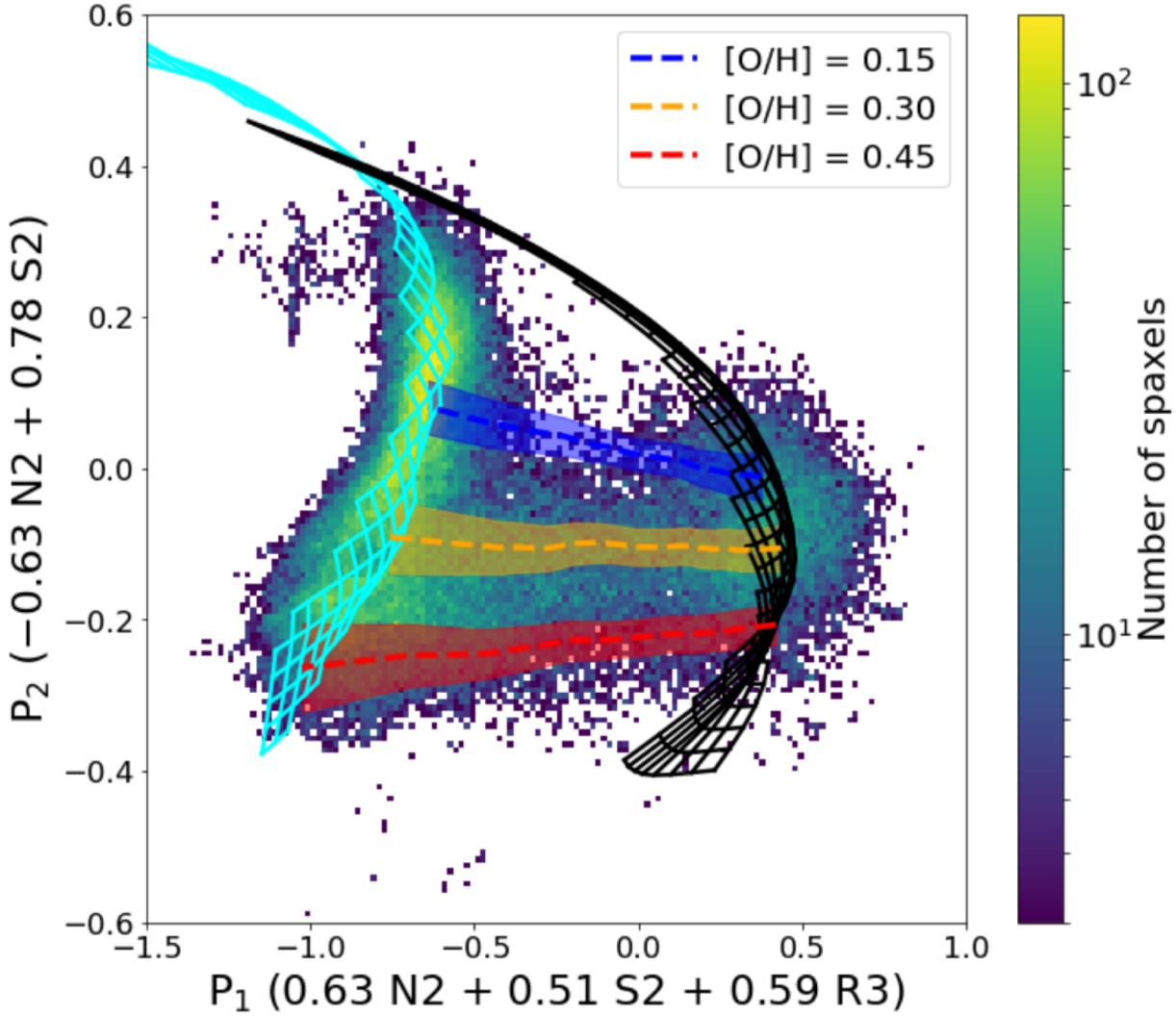

$$N2_{obs} = \log\left(\frac{([N\ II]/H\alpha)_{AGN} + i\ ([N\ II]/H\alpha)_{SF}}{1+i}\right),$$

. $i \equiv H\alpha_{SF}/H\alpha_{AGN}$.

Figure 9. Examples of iso-metallicity line bundles constructed from the photoionization models. The dashed lines are the median trends of line bundles with different metallicities. The colored shaded regions represent the projected areas within one stander deviation from the median along the vertical axis.

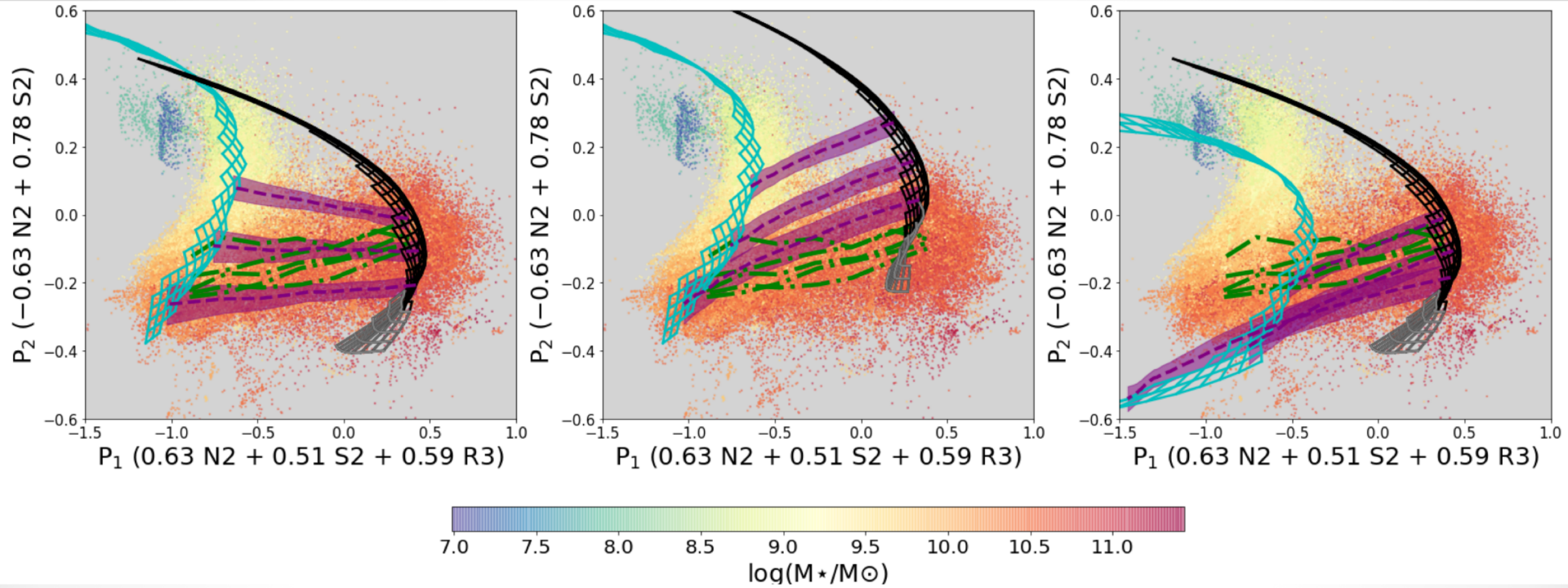

Штрих-пунктир – *линии* постоянной массы.
Штрих – *линии* постоянной металличности.
Слева – разные зависимости N/O vs O/H (Dopita+2013 и Groves+2004), справа и в центре – одинаковые.

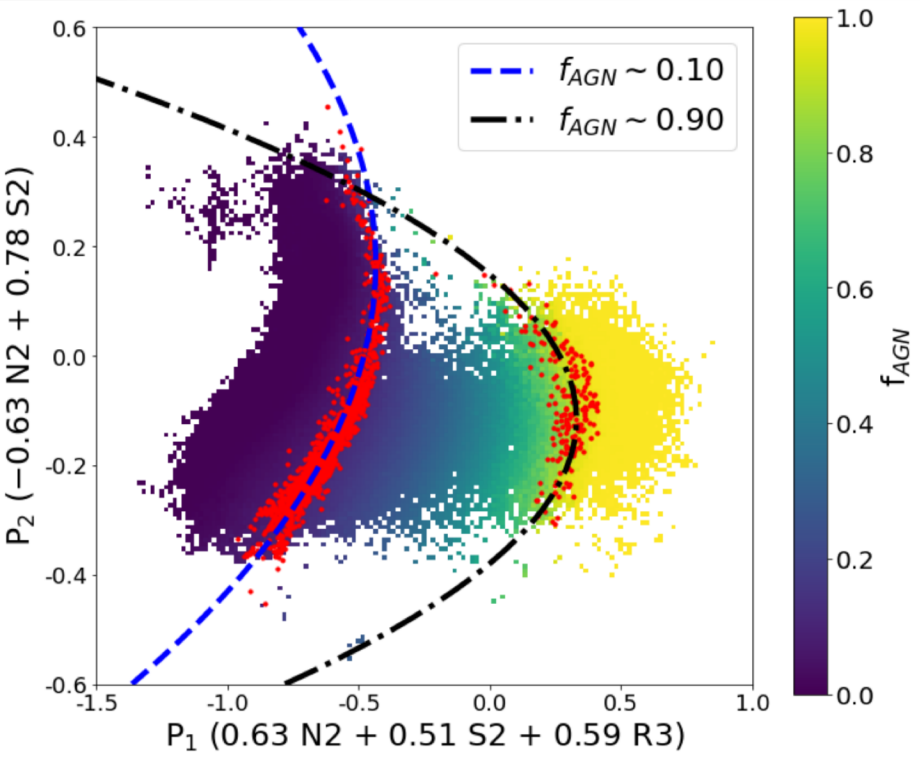

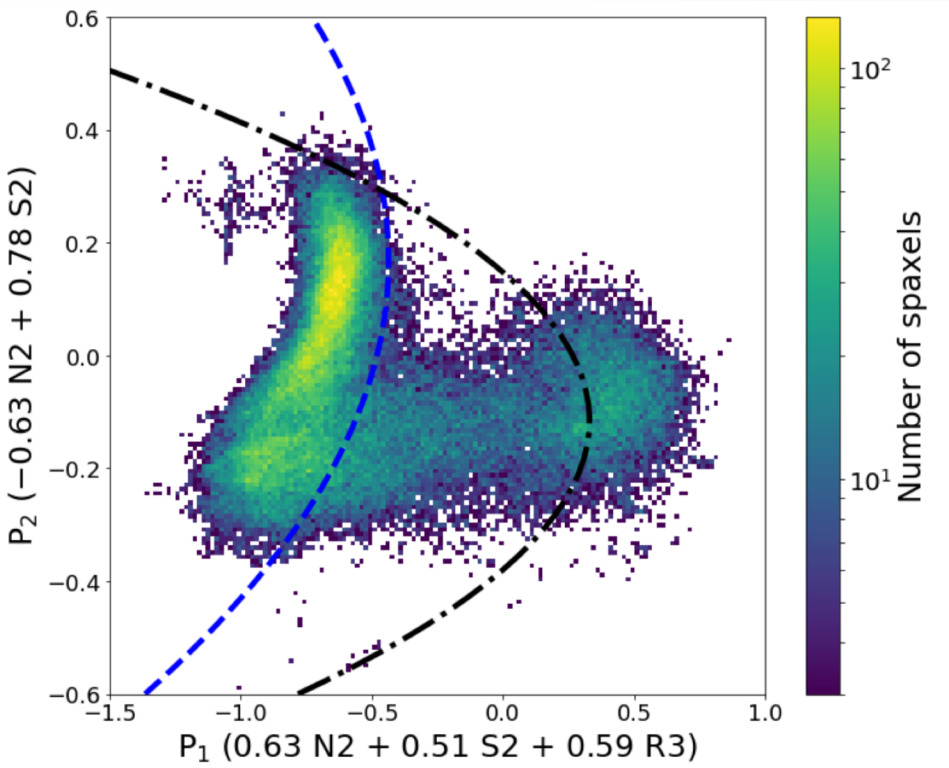

F_AGN – доля вклада AGN в общую ионизацию.

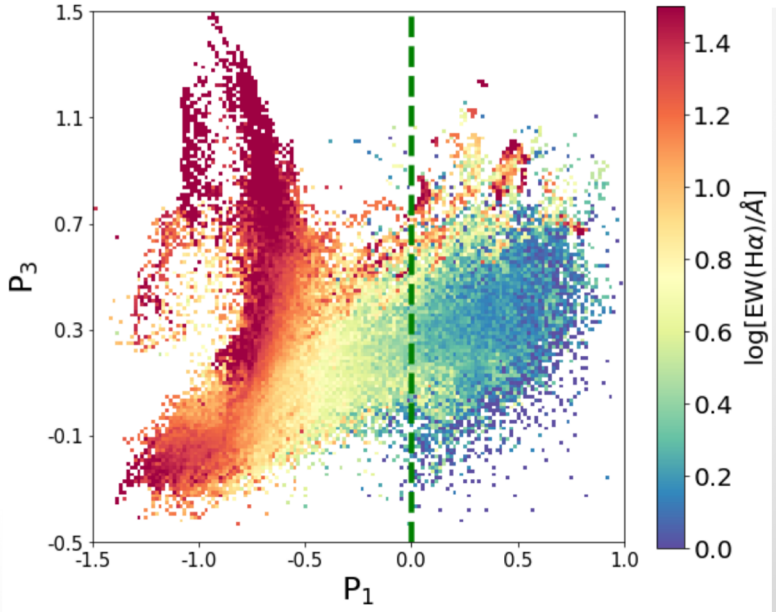

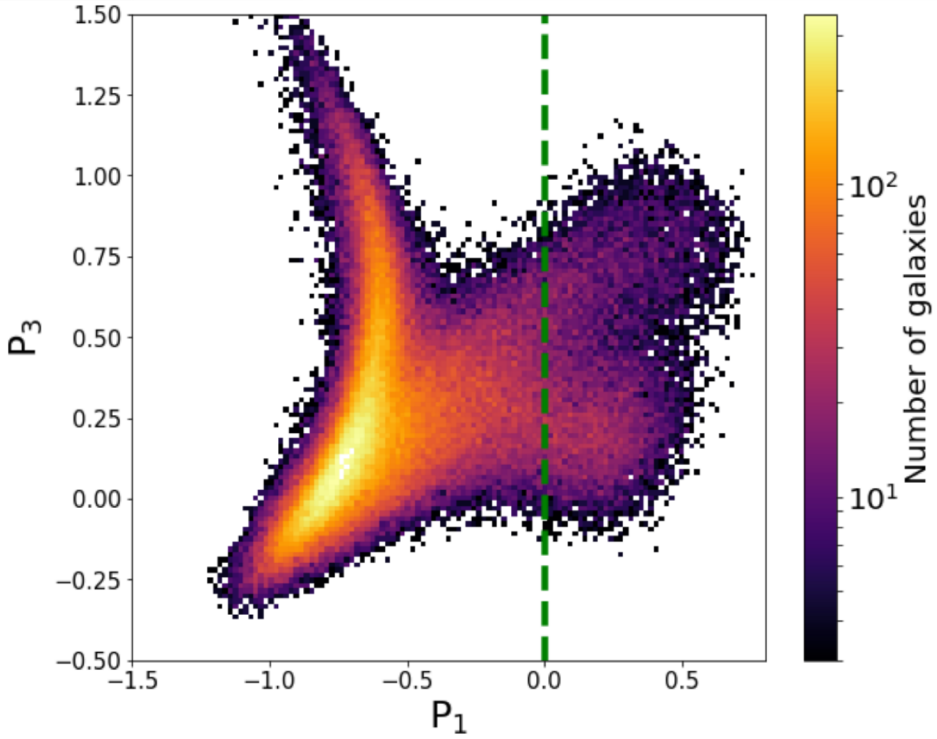

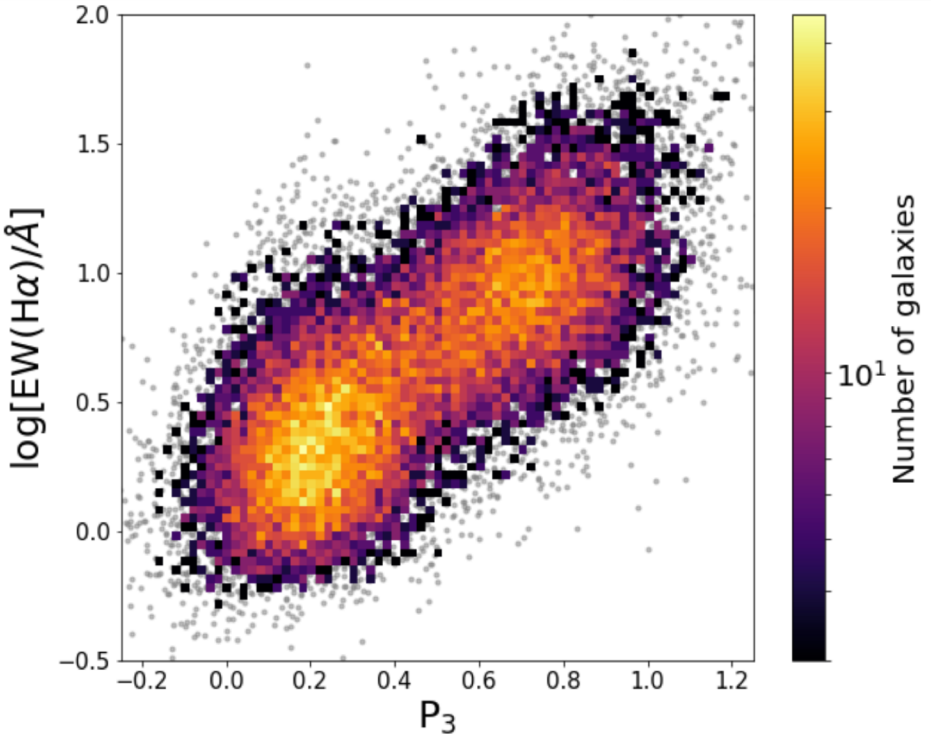

Хорошо разделяются AGN и LINER

$$P_3 = -0.46\ \mathrm{N2} - 0.37\ \mathrm{S2} + 0.81\ \mathrm{R3}.$$

$$P_1 = 0.63\ \mathrm{N2} + 0.51\ \mathrm{S2} + 0.59\ \mathrm{R3},$$